Journal of Inorganic Biochemistry 226 (2022) 111663

Contents lists available at ScienceDirect

Journal of Inorganic Biochemistry

journal homepage: www.elsevier.com/locate/jinorgbio

Distinct mechanism of action for antitumoral neutral cyclometalated Pt (II)-complexes bearing antifungal imidazolyl-based drugs

Natalia Fernández-Pampín [a,1], Mónica Vaquero [a,1], Tania Gil [a], Gustavo Espino [a], Darío Fernández [b,c], Begoña García [a], Natalia Busto [a,*]

[a] Departamento de Química, Facultad de Ciencias, Universidad de Burgos, Plaza Misael Bañuelos s/n, 09001 Burgos, Spain
[b] Departamento de Ciencias de la Salud, Facultad de Ciencias de la Salud, Universidad de Burgos, Paseo de los Comendadores, s/n, 09001 Burgos, Spain
[c] Consejo Nacional de Investigaciones Científicas y Técnicas, CONICET, Godoy Cruz 2290, C1425FQB, Buenos Aires, Argentina

ARTICLE INFO

Keywords:
Cyclometalated platinum(II) complexes
Clotrimazole
Bifonazole
Reactive oxygen species (ROS)
Antitumoral

ABSTRACT

Three neutral Pt(II) complexes containing 1-Methylimidazole and the antifungal imidazolyl drugs Clotrimazole and Bifonazole have been prepared. The general formula of the new derivatives is [Pt(κ^2-(*C^N*)Cl(**L**)], where *C^N* stands for ppy = 2-phenylpyridinate, and **L** = 1-Methylimidazole (**MeIm**) for **[Pt-MeIm]**; **L** = Clotrimazole (**CTZ**) for **[Pt-CTZ]** and **L** = Bifonazole (**BFZ**) for [**Pt-BFZ**]). The complexes have been completely characterized in solution and the crystal structures of [**Pt-BFZ**] and [**Pt-CTZ**] have been resolved. Complexes **[Pt-MeIm]** and **[Pt-BFZ]** present higher cytotoxicity than cisplatin in SW480 (colon adenocarcinoma), A549 (lung adenocarcinoma) and A2780 (ovarian cancer) cell lines. **[Pt-MeIm]** shows the highest accumulation in A549 cells, in agreement with its inability to interact with serum albumin. By contrast, **[Pt-CTZ]** and **[Pt-BFZ]** interact with serum proteins, a fact that reduces their bioavailability. The strongest interaction with bovine serum albumin (BSA) is found for **[Pt-BFZ]**, which is the least internalized inside the cells. All the complexes are able to covalently interact with DNA. The most cytotoxic complexes, **[Pt-MeIm]** and **[Pt-BFZ]** induce cellular accumulation in G0/G1 and apoptosis by a similar pathway, probably involving a reactive oxygen species (ROS) generation mechanism. **[Pt-BFZ]** turns out to be the most efficient complex regarding ROS generation and causes mitochondrial membrane depolarization, whereas **[Pt-MeIm]** induces the opposite effect, hyperpolarization of the mitochondrial membrane. On the contrary, the least cytotoxic complex, **[Pt-CTZ]** cannot block the cell cycle or generate ROS and the mechanism by which it induces apoptosis could be a different one.

1. Introduction

Clotrimazole (CTZ) and Bifonazole (BFZ) are well known antifungal agents used in mycotic infections like athlete's foot, vulvovaginal and oropharyngeal candidiasis, among others [1,2,3]. Due to the high efficiency and the unremarkable side effects of CTZ [4], this drug was tested against other infectious diseases (Malaria (*Plasmodium spp.*) and Chagas (*Trypanosoma cruzi*)) and cancer

In 1995, in vitro inhibition of tumor growth was described for melanoma and glioblastoma cells treated with CTZ and BFZ. This inhibitory effect is a consequence of their activity as calmodulin inhibitors [5]. Subsequently, these drugs have also been reported as inhibitors of the glycolytic enzymes [6]. Indeed, they prevent binding of kinases to the external membrane of mitochondria avoiding the phosphorylation of hexoses and accelerating the cellular apoptosis. This activity has been observed in different tumor cell lines (breast, cervical, prostate and melanoma cancer cell lines among others) [5,6].

Coordination of drugs to transition metals is a strategy that intends enhancing their biological activity and allows reducing the side effects or modifying their mechanism of action. Several Ru(II) and Ru(III) complexes bearing CTZ with biological activity as antiparasitic [7,8,9,10,11,12,13,14,15], antifungal [7,13,16], antitumoral [17,18] and antibacterial [19] agent and other metal complexes containing Au (I) [20], Ag(I) [21], Pd(II) [22], Mn(I) [23], Mn(II) [24], Cu(II) [20,23,25,26], Co(II) [23,24,25], Zn(II) [23,24,25,27], and Ni(II) [23,24,25] have been described in the literature, although there are

* Corresponding author.
E-mail address: nbusto@ubu.es (N. Busto).
[1] N. F—P and M. V. contributed equally. The manuscript was written through contributions of all authors. All authors have given approval to the final version of the manuscript.

https://doi.org/10.1016/j.jinorgbio.2021.111663
Received 21 September 2021; Received in revised form 4 November 2021; Accepted 5 November 2021
Available online 11 November 2021

scarce examples of Pt(II)-CTZ complexes and no examples of Pt(II)-BFZ derivatives.

The first clotrimazole-Pt(II) complex $K_2[PtCl_4(CTZ)_2]$ was described by Sánchez-Delgado and Urbina [8] and tested as antiparasitic agent against *Trypanosoma cruzi* with similar activity than $[Ru(bpy)(CTZ)_3](PF_6)_2$ (50 % of inhibition). Following with this strategy, Navarro et al., described the CTZ-platinum(II) complexes, *cis* and *trans*-$[PtX_2(CTZ)_2]$ (X= I and Cl), that present antitumoral activity [8,28]. The authors tested their activity against six tumor cell lines (prostate, pancreas, breast and colon among others) observing that both complexes showed lower cytotoxicity than cisplatin but higher than transplatin. DNA is identified as the biological target for these complexes, interacting by minor-groove [28].

Organometallic Pt(II) complexes containing monodentate N-donor ligands or cyclometalated ligands that can modify their anticancer mechanism of action have been recently reported [29,30,31] being DNA and serum proteins the most common targets. Several neutral cyclometalated complexes described in the literature displayed a different antiproliferative mechanism to DNA binding, being reactive oxygen species (ROS) generation a suitable strategy to induce programmed cell death in anticancer therapy [32,33].

Among the neutral cyclometalated complexes, we have synthesized a family of chiral neutral cyclometalated platinum(II) complexes with general formula $[Pt(\kappa^2\text{-}(C\hat{}N))Cl(\kappa^1\text{-}(\mathbf{L}))]$ where C^*N* = 2-phenylpyridinate and **L** stands for 2-(2-Pyridyl)benzimidazole derived ligands functionalized with CH_2-Ar (Ar = phenyl, naphtyl and pyrenyl) moieties on the imidazole fragment [34]. These neutral complexes were tested as antiproliferative drugs in SW480 cancer cell lines, being the complex with the unfunctionalized 2-(2-Pyridyl)benzimidazole ligand the most cytotoxic complex in spite of that DNA was not its biological target.

The antitumor neutral platinum complex, [Pt(II)(cis-[bis-(NHC)Cl (Cl)], containing a N-heterocyclic carbene (NHC, being NHC = 1,3-dibenzylimidazol-2-ylidene) showed a strongly interaction with DNA in vitro [35]**.** moreover, this complex reduced the mitochondrial membrane potential and also increased the cellular ROS levels. As a consequence, this complex showed cytotoxicity in 518A2 melanoma cells.

On the other hand, highly cytotoxic neutral cationic platinacycles based on bidentate phosphines were active against several breast and colon cancer cells. Their biological activity is related to ROS generation instead of DNA covalent binding [36].

Taking into account the above described precedents, the antitumoral activity of the imidazolyl antifungical agents CTZ and BFZ, the scarce examples of Pt(II)-CTZ complexes and the lack of Pt(II)-BFZ complexes, we tackle the synthesis of new neutral cyclometalated Pt(II) complexes bearing imidazolyl antifungal agents CTZ and BFZ, and 1-Methylimidazole (MeIm) as a model imidazolyl ligand. It worth mentioning that [Pt-MeIm] was previously tested in leukaemia tumor with promising results [34].

The coordination of the monodentate imidazolyl ligands to platinum could increase the cytotoxicity of the complexes respect to the free imidazolyl ligands, and the cyclometalated ligand ppy^- could confer interesting properties that could modify the mechanism of action of the classical Pt(II)-complexes avoiding tumor resistance.

2. Experimental Section.

2.1. General synthetic procedure for the Pt(II) complexes

Platinum precursor $[Pt(\kappa^2\text{-}(ppy)Cl(\kappa^1\text{-}(Hppy)]$ where ppy = 2-phenylpyridinate and Hppy = 2-phenylpyridine named as **[Pt-0]** (0.185 mmol) and the corresponding imidazolyl ligand (**MeIm**, 0.222 mmol; **CTZ**, 0.203 mmol and **BFZ** 0.185 mmol) were dissolved in 20 mL of DMF and the mixture was stirred for 24 h at 65 °C. The solvent was evaporated under reduced pressure, washed under stirring with Et_2O (2 × 7 mL) filtered and dried under vacuum. Detailed synthetic procedures and characterization of the complexes are compiled in the Supporting Information.

2.2. X-ray crystallography

Data collection and refinement parameters for **[Pt-CTZ]** and **[Pt-BFZ]** are summarized in Tables SI1 in the Supporting Information. A single crystal of the complexes was coated with high-vacuum grease, mounted on a glass fiber, and transferred to a Bruker SMART APEX CCD-based diffractometer equipped with a graphite-monochromated Mo Ka radiation source (λ = 0.71073). The highly redundant data sets were integrated with SAINT [37] and corrected for Lorentzian and polarization effects. The absorption correction was based on the function fitting to the empirical transmission surface as sampled by multiple equivalent measurements with the program SADABS [38]. The software package WingX [39] was used for space-group determination and structure solution, and OLEX 2 1.2.10 [40] was used for refinement by full-matrix least-squares methods based on F2. A successful solution by direct methods provided most non-hydrogen atoms from the E map. The remaining non-hydrogen atoms were located in an alternating series of least-squares cycles and difference Fourier maps. All non-hydrogen atoms were refined with anisotropic displacement coefficients. Hydrogen atoms were placed by using a riding model and included in the refinement at calculated positions. CCDC 2091796 (**[Pt-CTZ]**) and 2,091,795 (**[Pt-BFZ]**) contain the supplementary crystallographic data for this paper. These data are provided free of charge by The Cambridge Crystallographic Data Centre.

2.3. General procedure of stability by NMR spectroscopy

Stability in *DMSO-d_6:* Complexes were dissolved in DMSO-d_6 (300 μL, 1.42×10^{-3} M), and ^{1}H NMR spectra were recorded over 24 h in a 400 MHz spectrometer. *Stability in H_2O (3% DMSO)*: Complexes were dissolved first in DMSO-d_6 (150 μL) and water was added (4.850 mL, 1.5×10^{-2} M), ^{1}H NMR spectra were recorded over 24 h in a 300 MHz spectrometer. *Addition of $AgNO_3$:* Over a solution coming from the stability in H_2O (3% DMSO), $AgNO_3$ was added and the ^{1}H NMR spectra were recorded after 24 h and 48 h in a 300 MHz spectrometer.

2.4. General procedure of stability by HR-MS ESI spectroscopy

Samples of the complexes Pt(II) complexes were prepared in NaCaC (2.5 mM, pH = 7, 3% of DMSO) in concentrations of 100 ppm. The sample was injected after 24 h in solution in a 6545 Q-TOF (Agilent; V_{inj} = 0.1 μL). Mobile phase: H_2O-formic acid/MeOH (30:70) (0.1% of formic acid). Flow: 0.1 mL/min.

2.5. Cell culture

SW480 (colon adenocarcinoma) and A549 (lung carcinoma) cells from the ECACC (European Collection of Authenticated Cell Cultures, Salisbury, UK) were cultured in Dulbecco's Modified Eagle's Medium (DMEM) and A2780 (ovarian carcinoma) cells, also from the ECACC, were cultured in Roswell Park Memorial Institute (RPMI-1640). DMEM and RPMI were supplemented with 10% fetal bovine serum (FBS) and 1% amphotericin-penicillin-streptomycin solution (all from Sigma Aldrich). Cell were maintained at 37 °C in a humidified atmosphere containing 5% CO_2.

2.6. MTT antiproliferative assay

Cell proliferation was determined by the 3-(4, 5-dimethylthiazol- 2-yl)-2, 5-diphenyltetrazolium bromide (MTT) assay (Sigma Aldrich) using the following protocol: SW480 were seeded at a density of 1×10^4, A549 cells at 5×10^3 and A2780 at 2×10^4 cells per well in 96 well plates. After 24 h of incubation, cells were treated with different concentrations of the complexes under study for other 24 h. Then, treatment

was removed, and cells were incubated for 3 h with 100 μL of MTT (5 mg/mL) in culture medium at 37 °C and 5% CO_2. Then, 100 μL of solubilizing solution (10% SDS (*sodium* dodecyl sulfate) and 0.01 M HCl) was added to each well for dissolving the formazan crystals. Finally, plates were incubated overnight at 37 °C with soft agitation, and absorbance was measured at 590 nm using a microplate reader (Cytation 5 Cell Imaging Multi-Mode Reader -Biotek Instruments, USA). Four replicates per dose were included in each experiment and at least two independent experiments were performed. Then, half-maximal inhibitory concentration (IC_{50}) values were calculated using the GraphPadPrism Software Inc. (version 6.01) (USA). Phototoxicity experiments were carried out as previously described [41].

2.7. Cellular uptake

A549 cells were seeded in 12 well plates at a density of 1.5×10^5 cells in 2 mL of culture medium per well. Cells were treated with 2 μM of the tested drugs and incubated for 24 h. Then, cells were washed twice with DPBS (Dulbecco's Phosphate Buffered Saline), harvested and centrifuged. The pellets were resuspended in 1 mL of DPBS and 10 μL per sample were used to count the cells in an automated cell counter (TC20 – Biorad). Then, samples were digested with 65% HNO_3 at room temperature during 24 h for ICP-MS. Finally, solutions were analyzed in an 8900 Triple Quadrupole ICP-MS (Agilent Technologies).

2.8. Binding to serum albumin and DNA

Bovine serum albumin (BSA) as crystallized and lyophilized powder was dissolved in double deionized water from a Puranity TU system (VWR) and its concentration was spectrophotometrically determined ($\varepsilon_{278\ nm}$ = 45,000 M^{-1} cm^{-1}) [42]. Calf thymus DNA (ctDNA) as lyophilized sodium salt was dissolved in double deionized water and sonicated, producing short polynucleotide fragments (ca. 1000 base pairs). The molar DNA concentration was spectrophotometrically determined ($\varepsilon_{260\ nm}$ = 13,200 M^{-1} cm^{-1}) and expressed in base pairs [43]. Plasmid pUC18 (2686 bp) was extracted from *Escherichia coli* DH5α and purified by a HP Plasmid Midi kit (Omega Biotek, VWR). Sodium cacodylate, $(CH_3)_2AsO_2Na$, from now named NaCaC, was used as a buffer solution to keep pH = 7.0. All these reagents were purchased from Sigma Aldrich. Measurements of pH were made by a Metrohm 713 pH-meter equipped with a combined glass electrode.

2.9. Native polyacrylamide gel electrophoresis (PAGE) of bovine serum albumin (BSA)

PAGE experiments were done after overnight incubation at 37 °C of 1 μM BSA in the absence or in the presence of different concentrations of the Pt complexes. Then, 5 μL of sample buffer 2× 0.01% bromophenol blue and 20% glycerol in Tris HCl buffer (0.5 M, pH 6.8) were added to 5 μL of the sample solutions and loaded onto 10% polyacrylamide gels. Gels were run in native PAGE buffer (250 mM Tris Base, 1.92 M glycine, pH = 8.3) at 6.6 V/cm for 6 h at 4 °C to avoid thermal denaturation of the protein. Finally, gels were stained with Coomassie brilliant blue R-250 and visualized with a Gel Doc XR+ Imaging System (Bio Rad).

2.10. Agarose gel electrophoresis of plasmid DNA (pUC18)

Agarose gel electrophoresis of plasmid was performed after overnight incubation at 37 °C of the plasmid (3.7 μM, base pairs) in the presence of different concentrations of the Pt(II) complexes in 2.5 mM NaCaC, pH = 7.0. Samples were loaded onto 1% agarose gel and electrophoresis was run at 6.5 V/cm during 150 min. After the run, the gel was stained with a solution of ethidium bromide 1 μg/mL in Tris-borate-EDTA (TBE) 1× for 30 min. Finally, the gel was visualized in a Gel Doc XR+ Imaging System (Bio-Rad).

Data Analysis. All data were expressed as mean ± standard deviation (SD). Statistical significance was evaluated using by statistical analysis performed with GraphPadPrism Software Inc. (version 6.01, USA).

2.11. Circular dichroism (CD)

CD spectra were recorded on a MOS-450 Biologic spectrometer (Claix, France) for samples at a Pt(II) complex/BSA concentrations ratio of 5 and at Pt(II) complex/ctDNA (calf thymus DNA) concentrations ratio of 1 incubated overnight, in 2.5 mM NaCaC buffer at pH = 7.0 and T = 25 °C.

2.12. Intracellular reactive oxygen species (ROS) generation

A549 cells were seeded in a clear bottom black side 96 well plate at a density of 3×10^4 cells per well and incubated for 24 h. Then, media was removed and for ROS quantification by the probe 2′,7′-dichlorodihydrofluorescein diacetate (H_2DCFDA), 100 μL of 25 μM of H_2DCFDA in DMEM without phenol-red was added to each well. Cells were incubated for other 30 min and then, cells were treated with 100 μL of the vehicle and with the corresponding Pt(II) complex with the required concentration to obtain a final concentration equal to the IC_{50} value. Cells treated with 20 μM of tetrabutylammonium hydroxide (TBH) were included as positive control. After 2 h of treatment, cells were washed twice with DPBS and emission was measured at λ_{em} = 530 nm with λ_{exc} = 490 nm during 2 h in a microplate reader (Cytation 5 Cell Imaging Multi-Mode Reader -Biotek Instruments, USA). Measurements at 4 h after treatment were selected at the final point for data analysis. Cell images were also taken, and the collected results were corrected by the number of cells. Two independent experiments with 4 replicates per treatment were performed. For the dihydroethidium (DHE) assay, instead of H_2DCFDA, cells were incubated with 0.5 μM of DHE (dihydroethidium) for 20 min. Then, cells were washed twice with phosphate buffer saline (PBS) and fluorescence intensity was measured after 2 h at λ_{em} = 535 nm with λ_{exc} = 635 nm in a microplate reader (Cytation 5 Cell Imaging Multi-Mode Reader -Biotek Instruments, USA). The emission of each well was corrected by the number of cells. Results are expressed as the mean and standard deviation of two independent experiments with 4 replicates per dose.

The levels of cytosolic superoxide anion in untreated A549 cells and after 2 h of treatment with the vehicle (0.5% DMSO) of the imidazolyl-Pt (II) complexes were also evaluated by flow cytometry. For this aim, A549 cells were seeded at a density of 30,000 cells/well and incubated for 24 h. Then, cells were incubated with 1 μM DHE during 20 min in DMEM without phenol red. Then, cells were washed twice with PBS and treated at the IC_{50} values of the Pt(II) complexes under study. After 2 h of incubation, cells were harvested, washed with PBS, and collected in 100 μL of PBS. Finally, cells were analyzed by flow cytometry (NovoCyte Flow cytometer, ACEA Biosciences, Inc., USA). Two replicates per experimental condition and two independent experiments were performed and analyzed by NovoExpress 1.4.0 Software.

2.13. Mitochondrial membrane potential (MMP) assay by TMRM (tetramethyl rhodamine methyl ester)

The effect of the imidazolyl Pt(II)-complexes on the MMP of A549 cells was evaluated by means of tetramethyl rhodamine methyl ester (TMRM). A549 cells were seeded in a clear bottom black side 96 well plate at a density of 3×10^4 cells per well and incubated for 24 h. Then, media was removed and replaced by 100 μL of assay buffer (25 mM D-glucose, 80 mM NaCl, 75 mM KCl, 25 mM Hepes (4-(2-hydroxyethyl)-1-piperazineethanesulfonic acid), pH = 7.4) and cells were treated with the vehicle (0.5% DMSO) and the Pt(II) complexes at their IC_{50} values during 1 h. Then, 10 μL of TMRM (2 μM) were added and after 15 min of incubation at room temperature and light protected, cells were washed twice with PBS. Afterwards, 100 μL of PBS were added and fluorescence of TMRM was measured after 15 min at λ_{em} = 535 nm with λ_{exc} = 590

nm in a microplate reader (Cytation 5 Cell Imaging Multi-Mode Reader -Biotek Instruments, USA). The fluorescence intensity of each well was corrected by the corresponding number of cells. Two independent experiments with 4 replicates per treatment were performed.

2.14. Cell cycle arrest

To study the perturbations in the cell cycle of A549 cells induced by platinum complexes, cells were stained with propidium iodide (PI) and analyzed by flow cytometry. Briefly, 1.5×10^5 cells per well were seeded in 6 well plates. Cells were treated at the IC_{50} value for each complex. Cells without any treatment and vehicle-treated cells (0.5% DMSO) were used as control. After 24 of treatment, cells were harvested and centrifuged, resuspended in cold PBS and finally fixed in 70% EtOH (CH_3CH_2OH) overnight at 4 °C. After fixation, samples were treated with a solution containing 0.1 mg/mL PI, 0.1 mM EDTA *(ethylenediaminetetraacetic acid)* and 0.1% Triton- × 100 in PBS to permeabilize and stain cells, and with RNAse (2 mg/mL) for 30 min in ice and protected from light. Finally, cells were analyzed using the NovoCyte Flow cytometer (ACEA Biosciences, Inc., USA). Cell cycle distribution was evaluated by NovoExpress 1.4.0 Software. Two replicates per experimental condition and three independent experiments were performed.

2.15. Apoptosis detection by flow cytometry

Apoptosis was evaluated by an Annexin V:FITC Assay Kit (Biorad) according to the manufacturer's instructions. Briefly, A549 cells were seeded at a density of 2×10^5 cells per well in 12 wells plates and incubated for 24 h. Then, cells were treated at the IC_{50} value for each complex. After other 24 h, cells were washed with cold PBS, harvested, and resuspended in binding buffer. Afterwards cells were stained with Annexin V:FITC conjugate, that is, annexin V conjugated with fluorescein isothiocyanate (FITC) during 10 min (light protected) at room temperature. Then, cells were washed with binding buffer, centrifuged, and resuspended in 190 μL of binding buffer, 10 μL of propidium iodide (PI) (20 μg/mL) were added just before data collection in a NovoCyte Flow cytometer (ACEA Biosciences, Inc., USA). 10,000 events were counted and analyzed by NovoExpress 1.4.0 Software. Two replicates and two independent experiments were performed.

3. Results and Discussion

3.1. Synthesis of the neutral cyclometalated Platinum(II) complexes

1-Methylimidazole (**MeIm**), Clotrimazole (**CTZ**) and Bifonazole (**BFZ**) are commercially available. All the complexes, isolated as pale-yellow solids, are air- and moisture- stable. Neutral Platinum(II) complexes **[Pt-MeIm]**, **[Pt-CTZ]** and **[Pt-BFZ]** of general formula [Pt(*ppy*)Cl(**L**)], being **L** = **MeIm**, **CTZ** and **BFZ**, respectively, and ppy = 2-phenylpyridinate, were synthesized by direct reaction of the platinum precursor [Pt(κ^2-(ppy)Cl(κ^1-(Hppy)] [34,44], from now **[Pt-0]** (Hppy = 2-phenylpyridine), in DMF at 65 °C (Scheme 1 and synthetic procedures in SI). Complex **[Pt-MeIm]** has been previously synthesized [45], but the synthetic procedure described herein avoids the synthesis of the intermediate [Pt(*ppy*)Cl(DMSO)], affording the desired **[Pt-MeIm]** complex in similar yields.

3.2. Characterization in solution and in solid state

3.2.1. Characterization in solution

Pt(II)-complexes were completely characterized in solution by NMR spectroscopy in $CDCl_3$, IR, elemental analysis as well as high resolution mass spectrometry, and, in the solid state, by X-ray diffraction of single crystal.

Spectroscopic data obtained for **[Pt-MeIm]** are in concordance with

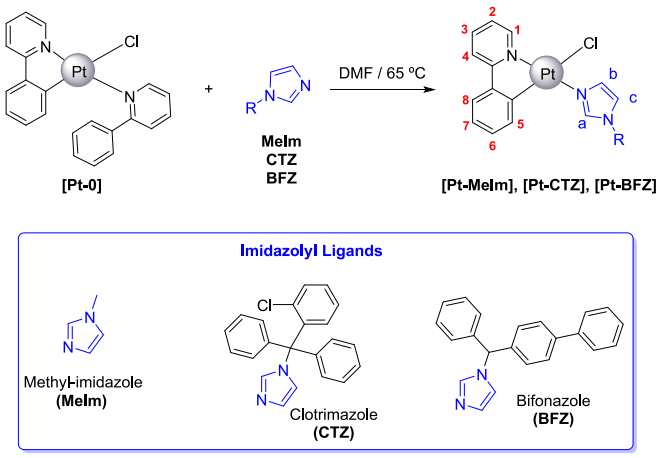

Scheme 1. Synthetic procedure for the neutral cyclometalated Pt (II) complexes.

those described by Esmaeilbeig et al. [45] (see characterization in S·I). ^{1}H NMR spectra of the Pt(II) complexes **[Pt-CTZ]** and **[Pt-BFZ]** showed characteristic satellites due to the expected ^{195}Pt—^{1}H couplings for the protons H1 ($J_{Pt\text{-}H}$ = 35–39 Hz) and H5 ($J_{Pt\text{-}H}$ = 45–47 Hz) of the 2-phenylpyridinate ligand and for the proton Ha ($J_{Pt\text{-}H}$ = 18–22 Hz) of the imidazolyl fragment (see spectra of **[Pt-BFZ]**, Figure SI1, as representative Pt(II) complex). The last feature corroborates the coordination of the imidazolyl ligands to the Platinum center. The HR-MS ESI(+) spectra recorded for the neutral cyclometalated Pt(II) complexes exhibited in each case a peak fully compatible with the respective cationic fragment $[Pt(C^N)(\mathbf{L})]^+$ (*m/z* ratio and isotopic pattern), which correspond to the loss of the chloride ligand (see characterization in Supporting information).

3.2.2. Solid state characterization

Suitable single crystals for X-ray structural determination were obtained for the complexes **[Pt-CTZ]** and **[Pt-BFZ]** by slow evaporation of a solution of the complexes in acetone. Both ORTEP diagrams are depicted in Fig. 1, selected bond lengths and angles with estimated standard deviations are gathered in, and crystallographic refinement parameters are given in the Supporting Information (Table SI1). Structure of the **[Pt-MeIm]** has been previously described by Esmaeilbeig et al. [45] (data are compiled in Table 1 for comparative purpose).

Complex **[Pt-CTZ]** crystallizes in the monoclinic space group $P2_1/c$ and shows four molecules in the unit cell, while **[Pt-BFZ]** crystallizes in a triclinic space group P-1 with two molecules in the unit cell which differ from each other in the orientation of the imidazole fragment, along with an acetone molecule. In both structures, the platinum center displays a slightly distorted square plane coordination geometry with a *trans*-N,N disposition for the N atom of the 2-phenylpyridinate ligand and the N atom of the imidazole fragment of the corresponding imidazolyl ligands. The Pt—N distances that define the distorted square planar

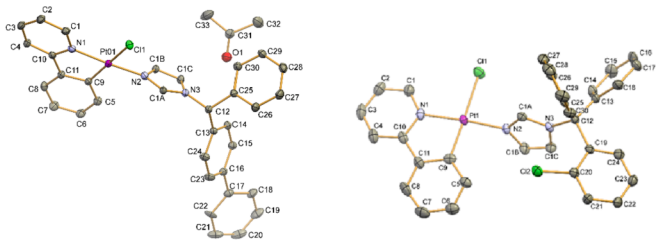

Fig. 1. ORTEP diagram for **[Pt-CTZ]** (left) and **[Pt-BFZ]** (right) forming part of the asymmetric units. Hydrogen atoms have been omitted for clarity. Thermal ellipsoids are shown at the 50% probability level.

Table 1
Selected bond lengths (Å) for the molecular structure of complexes **[Pt-CTZ]** and **[Pt-BFZ]**.

Distances (Å)	[Pt-MeIm] [45]	[Pt-CTZ]	[Pt-BFZ]	Angles (°)	[Pt-MeIm] [45]	[Pt-CTZ]	[Pt-BFZ]
Pt(01)-Cl(1)	2.4105(13)	2.3807(18)	2.3876(10)	N(2)-Pt(01)-Cl(1)	87.45(13)	87.72(15)	88.76(10)
Pt(01)-N(2)	2.026(5)	2.028(5)	2.028(4)	C(9)-Pt(01)-N(1)	81.3(2)	82.1(3)	81.51(15)
Pt(01)-C(9)	1.978(5)	1.967(6)	1.979(4)	N(1)-Pt(01)-Cl(1)	96.60(12)	96.31(16)	95.69(10)
Pt(01)-N(1)	2.017(4)	2.023(5)	2.013(4)	C(9)-Pt(01)-N(2)	94.9(2)	93.8(2)	94.67(15)

geometry present values of approx. 2 Å, as was described for **[Pt-MeIm]** (see Table 1) [45]. The Pt-Cl(1) distance (approx. 2.4 Å) observed for the complexes **[Pt-CTZ]** and **[Pt-BFZ]** are standard for a Pt—Cl bond in which the Cl^- are located in *trans* position to the sp^2 carbon of the 2-phenylpyridinate ligand [34,45,46,47,48,49]. The bite angles C(9A)-Pt(1)-N(1) for the Pt(II) complexes are around 81°, while the opposite angles N(2)-Pt(1)-Cl(1) present values of 87–88° (see Table 1).

The 3D-structures of **[Pt-CTZ]** and **[Pt-BFZ]** are stabilized by different spatial interactions. In the structure of **[Pt-CTZ]** a chloride atom of one molecule is involved in hydrogen bonding interactions with two hydrogen atoms (H3 and H4) of two ppy^- ligands that belong to two different molecules (see Figure SI2 and Table SI2). Besides, each molecule of **[Pt-CTZ]** participates in two chloride bond interactions C-Cl—C between the C20—Cl and C16 of a different molecule (See Figure SI3 and Table SI4). Additionally, two CH-π interactions are observed for the same molecule of **[Pt-CTZ]**, (see Figure SI4 and Table SI3). In the case of the complex **[Pt-BFZ]** the chloride atom is involved in hydrogen bonding intermolecular interactions with the H6 atom of a ppy^- of a neighbor molecule, the Ha and CH of another different neighbor molecule, and a H of a methyl group of the acetone molecule (see Figure SI5 and Table SI2). In addition, between the same molecules of **[Pt-BFZ]** different CH-π interactions are observed in the crystal structure. These interactions are resumed in the supporting information (Figure SI6, and Table SI3) along with the interactions in which one molecule of acetone is implicated (Figure SI7).

3.3. Stability in solution

First of all, the stability in solution of the Pt(II)-complexes in DMSO-d_6 (1.42 10^{-3} M, 300 μL) was studied over 24 h by ^{1}H NMR spectroscopy (the stock solutions of the complexes were stored in DMSO). The imidazolyl Pt(II) complexes showed a low degree of ligand dissociation after 24 h, 3% of dissociation of the **MeIm** for **[Pt-MeIm]**, 17% and 28% of the corresponding ligands for **[Pt-BFZ]** and **[Pt-CTZ]**, respectively (see Figures SI8-SI10). In any case, the substitution of the Cl^- anion by DMSO-d_6 was observed. This behavior was previously described for [Pt(*ppy*)Cl(Hpybzi)] derivatives [34]. The stability of the Pt(II) complexes in DMSO solution was also studied by UV measurements and the recorded spectra showed no changes during 24 h (Figure SI11).

Additional stability studies for the Pt(II) complexes were performed in D_2O/DMSO-d_6 (97:3) by monitoring the evolution of the ^{1}H NMR spectra during 24 h. DMSO-d_6 was used to ensure the complete dissolution of the complexes (see Figures SI12-SI14). Indeed, this solvent mixture is commonly employed in biological studies for water-insoluble metal complexes. Then, $AgNO_3$ was added to force the release of the chloride anion and the formation of the corresponding aqua-complex (aquation process). In particular, the ^{1}H NMR spectra of **[Pt-MeIm]** in a D_2O (3% DMSO-d_6) remained essentially unchanged over 24 h, confirming the stability of this complex in the medium (compare spectra a and b in Figure SI12). However, the addition of $AgNO_3$ gave place to a new set of signals, that we tentatively assigned to the aqua-complex [Pt(ppy)(D_2O)(**MeIm**)]$^+$ (compare spectra b, c and d in Figure SI12). This fact confirmed us that the chloride is still bound to the Pt center after 24 h in aqueous solution. A similar behavior is observed for **[Pt-CTZ]** and **[PT-BFZ]** complexes under analogous conditions. Hence, these two complexes are also stable in water solution (spectra a and b in Figure SI13 for **[Pt-CTZ]** and spectra a and b in Figure SI14 **[PT-BFZ]**). Furthermore, we could conclude that the aquation process did not take place in aqueous media.

The stability of the imidazolyl-Pt(II) complexes was also checked by HR-MS ESI spectrometry in buffered media (Sodium Cacodylate (NaCaC), 2.5 mM, pH = 7, 3% DMSO) (see experimental section). All the complexes are stable after 24 h of incubation in a solution of sodium cacodylate NaCaC (DMSO 3%; see NaCaC chromatogram in Figure SI15 and chromatograms of the Platinum complexes in Figures SI16 − SI18). Free ligands **MeIm**, **CTZ** and **BFZ** were not observed in any case.

3.4. Photophysical properties

UV–Vis absorption spectra of the neutral cyclometalated Pt(II) complexes were recorded in H_2O (3% DMSO) (10^{-5} M) and in acetonitrile solutions for comparison with other Pt(II) complexes described in the literature. The absorption spectra of the Pt(II)-imidazolyl complexes in H_2O present a broad band with the maximum located between 235 and 255 nm (Fig. 2, data in Table 2). These absorption bands could be attributable to singlet spin-allowed ligand centered transitions (π → π*, ^{1}LC) that takes place in both the imidazolyl (**MeIm**, **CTZ** and **BFZ**) and the ppy^- ligands. In the area between 373 and 433 nm, typical of the ^{1}MLCT transitions, the complexes present low intense bands, similar to those observed for related cyclometalated ppy-Pt complexes [45,50,51].

The absorption profile of the Pt(II) complexes did not present remarkable solvatochromism effects when comparing the spectra measured in aqueous solution with those recorded in acetonitrile (see Figure SI19 and Table SI5).

The photoluminescence properties of the complexes have been recorded in 10^{-5} M solutions in both deoxygenated H_2O (3% DMSO) (see Fig. 2, data in Table **2**) and acetonitrile (see Figure SI20, data in Table SI6).

In both solvent systems, the new cyclometalated Pt(II) complexes showed photoluminescence in the cyan-green hue under irradiation with λ_{exc} = 375 nm, absorption wavelength that corresponds to ^{1}MLCT transitions. The spectra profiles for the platinum complexes **[Pt-MeIm]** and **[Pt-CTZ]** are quite similar in both solvent systems with the maximum of the emission bands centered at 480 nm and 514 nm that are assigned to spin-allowed ^{1}MLCT and spin-forbidden and, for **[Pt-MeIm]** ^{3}MLCT (singlet to triplet dπ(Pt) → π*(N^N)), ^{3}LLCT (singlet to triplet, 3π(N^N) →π*(C^N)) and ^{3}LC (singlet to triplet 3π → π*) transitions.[51] The complex **[Pt-BFZ]** showed a different emission spectrum with broad emission bands (491 nm and 529 nm) and a plateau that

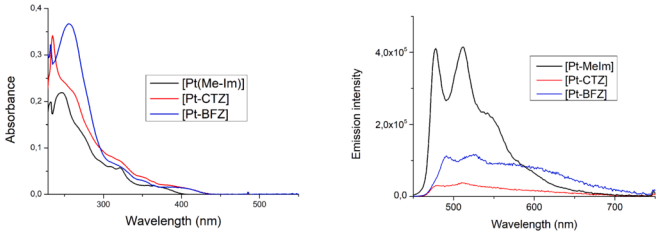

Fig. 2. Absorption (left) and emission (right) spectra in deoxygenated H_2O (3% DMSO) of the Pt(II) complexes (10^{-5} M).

Table 2
Electronic and photophysical data for the Pt(II) complexes in deoxygenated H_2O (3% DMSO, 10^{-5} M) at 25 °C.[a]

Complex	λ_{abs} (nm)/ ε 10^{-3} ($M^{-1}\cdot cm^{-1}$)		λ_{em} [nm]	$\Delta\lambda$ [nm][d]	ϕ_{PL} [%][c]	$\tau_{1/2}$ [ns][d]
	$\pi \rightarrow \pi^*$	MLCT				
[Pt-MeIm]	232(19.87), 247(21.90)◆, 322(5.71)^s	364(1.88)*	478,◆ 512◆	103, 137	6.43	3014
[Pt-CTZ]	235(34.13)◆, 235(21.81)^s, 322(7.13)^s	390(1.13)*	476, 510	101, 135	4.21	166
[Pt-BFZ]	232(37.45), 256(41.96)◆, 326^s(10.78), 355 (7.98)	392(6.75)*	491, 529, 602*	116, 154, 227	2.58	267

[a] λ_{exc} = 375 nm, (s) Shoulder, *Broad band, ◆= maximum.

enter into the red spectrum region centered at 602 nm. The spectrum of the complex in acetonitrile showed a great blue-shifted for the bands up to 54 nm. As for the excited state half lifetime,$\tau_{1/2}$, the complexes exhibited higher half-life times in H_2O (3% DMSO) (3 μs for **[Pt-MeIm]** , 166 ns and 267 ns for **[Pt-CTZ]** and **[Pt-BFZ]** , respectively, Table 2) than in acetonitrile (28.97 ns for **[Pt-MeIm]** , 28.90 ns for **[Pt-CTZ]** and 43.29 ns **[Pt-BFZ]** , see Table SI6). We should highlight here that **[Pt-MeIm]** is a phosphorescent complex in deoxygenated H_2O. The differences on the half-life times in both solvent systems are related to the stabilization of the excited state in protic polar solvents compared to those in acetonitrile solution [52]. Regarding to the photoluminescence quantum yields (ϕ_{PL}), the values decrease according the following sequence **[Pt-MeIm] > [Pt-CTZ] > [Pt-BFZ]** . Hence, **[Pt-MeIm]** exhibit the maximum value in both solvent systems (6.43% in H_2O (3% DMSO) and 15.81% in acetonitrile). Despite their emission properties, they have not been visualized inside the cells.

3.5. Biological behavior

3.5.1. Cytotoxicity of the Pt(II) complexes

The viability of the human cell lines A549 (lung adenocarcinoma), SW480 (colon adenocarcinoma) and A2780 (ovarian cancer) was studied after 24 h of treatment of the cells with the platinum complexes by means of the MTT assay (Table 3).

Our present studies have demonstrated that **[Pt-CTZ]** is the less cytotoxic complex whereas **[Pt-MeIm]** and **[Pt-BFZ]** are more active than cisplatin against all the studied tumor cells. While **[Pt-MeIm]** is the most active derivative in the SW480 cell line, **[Pt-BFZ]** is as cytotoxic as **[Pt-MeIm]** in the A549 and A2780 cells. Photoactivation of these Pt(II) complexes by UV (λ = 365 nm, 8 mW cm^{-2}) and blue (λ = 460 nm, 5.5 mW cm^{-2}) light irradiation have also been evaluated with negative results since no variation of the half maximal inhibitory concentration was observed.

3.5.2. Cellular uptake

After 24 h of exposure of lung adenocarcinoma A549 cells to 2 μM of the Pt-complexes, the values obtained for the cellular uptake by ICP mass spectrometry were compared with those observed for cisplatin (CDDP) (Fig. 3). **[Pt-MeIm]** was the most internalized compound in the A549 cells, in agreement with its high cytotoxic activity, in high extent than CDDP. By contrast, **[Pt-BFZ]** exhibits a low degree of accumulation in this cell line, lower than cisplatin, in spite of its high cytotoxicity. The opposite trend is observed for **[Pt-CTZ]** , which displays a high cellular uptake inside A549 cells although is almost inactive.

Table 3
IC_{50} (μM) of the Pt(II) complexes in different cell lines after 24 h of exposure time.

	SW480	A549	A2780
[Pt-MeIm]	11.6 ± 3.5	22.6 ± 1.8	7.0 ± 0.6
[Pt-CTZ]	61.5 ± 4.0	50.6 ± 1.6	68.7 ± 4.0
[Pt-BFZ]	38.3 ± 3.3	19.0 ± 1.4	6.1 ± 0.4
cisplatin	45.1 ± 9.1	38.8 ± 1.2	10.5 ± 0.5

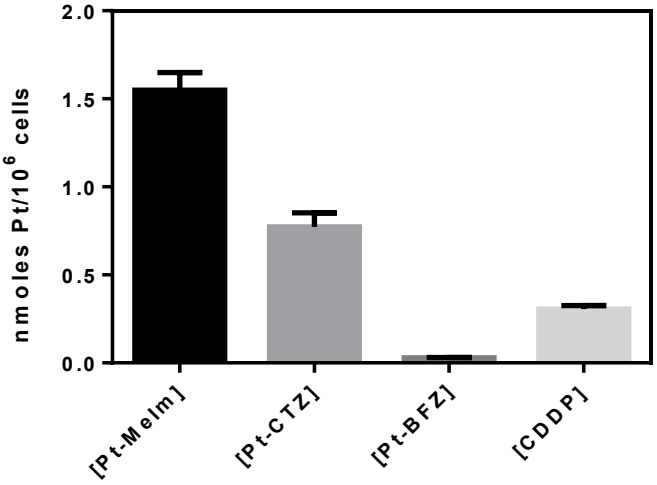

Fig. 3. Metal accumulation determined by ICP-MS in A549 cells after 24 h of treatment with 2 μM of the Pt complexes.

3.5.3. Binding studies of the Pt(II) complexes to BSA and DNA

Cellular uptake depends, among other factors, on drug sequestration by plasma proteins before reaching the tumor cells. Since human serum albumin (HSA) is the main protein of blood and cerebrospinal fluid and plays a key role in bio-distribution of essential metal ions and a large variety of endogenous and exogenous molecules [53], HSA binding studies are essential to understand ADME (Absorption, Distribution, Metabolism, and Excretion) properties of the drugs [54]. Bovine serum albumin (BSA) is often used as a model for HSA binding studies due to its similarity and its lower cost. It is known that upon cisplatin administration, more than 90% of the Pt is covalently bound to the plasma proteins as albumin, transferrin, and γ-globulin [55]. Therefore, native polyacrylamide gel electrophoresis (PAGE) experiments over BSA incubated with different ratios of the imidazolyl-Pt complexes were performed (Fig. 4). **[Pt-BFZ]** strongly affects the BSA native conformation at low concentration of this complex (**[Pt-BFZ]** /[BSA] = 25). On the contrary, **[Pt-CTZ]** only affects BSA conformation at high concentration ratios (**[Pt-CTZ]** /[BSA] ratios of 25 and 50) and in a less extent than **[Pt-BFZ]** .

In order to confirm this interaction, circular dichroism experiments of BSA incubated overnight in presence of the cyclometalated Pt(II)-complexes were performed (Figure SI21). No significant differences in the BSA intrinsic band (centered at 220 nm) were observed for **[Pt-MeIm]** . However, **[Pt-BFZ]** and **[Pt-CTZ]** induce conformational

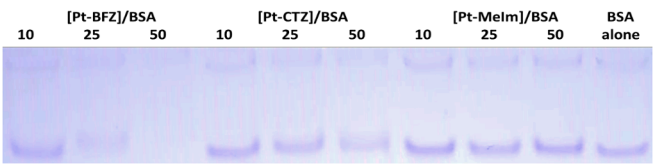

Fig. 4. Native PAGE of BSA incubated overnight with Pt-complexes. C_{BSA} = 1.5 μM, [Pt-complex]/[BSA] ratios: 10, 25 and 50, C_{DMSO} = 0.2%.

changes in the BSA structure according to the native PAGE results. These results allowed us to explain qualitatively the large differences in metal accumulation observed in the uptake studies (see Fig. 3). The higher the interaction of the complexes with BSA, the lower their accumulation inside cells.

Although the antitumoral activity of **[Pt-MeIm]** has been previously described in leukaemia tumor cells [45], there is no evidence of its interaction with DNA. To explore the potential interactions of the Pt(II)-imidazolyl complexes with DNA they were incubated with the plasmid DNA (pUC18) at 37 °C overnight and, then, their electrophoretic mobility through an agarose gel was evaluated (Fig. 5). The presence of the imidazolyl-Pt(II) complexes affects the DNA migration in a concentration dependent manner, suggesting conformational modifications in the standard double stranded DNA. All of them induced condensation of the Open Circular (OC) band and retardation in the migration of the Super-coiled (SC) band. These changes are compatible with DNA covalent binding.

In order to confirm these results, Circular Dichroism (CD) experiments were performed. The Pt(II)-complexes modified the molar ellipticity of the DNA double helix as a function of the incubation time (Figure SI22). This feature together with the observed changes in the migration patterns of the electrophoresis experiments indicate a covalent Pt-DNA binding. More specifically **[Pt-MeIm]** induces the most pronounced structural changes in DNA conformation, while **[Pt-CTZ]** causes the lowest impact in DNA conformation. Therefore, the covalent Pt-DNA binding could be one of the mechanisms of cytotoxicity operating in the case of these Pt-complexes. Nevertheless, it is insufficient to justify the paradoxical high cytotoxicity of **[Pt-BFZ]** considering its reduced cellular uptake and moderate interaction with DNA.

3.5.4. *ROS production*

The generation of reactive oxygen species (ROS) is often involved in the mechanism of action of many cytotoxic agents [56], some Pt(II) derivatives among them [35,57,58,59]. Although ROS play important roles in living cells, an abnormal increase of these species can generate damage on DNA, lipids and proteins. These oxygen species can produce oxidative stress altering the redox status of the tumor cells and triggering their programmed dead [60].

Thus, the levels of intracellular ROS in A549 tumor cells was measured by means of two different probes: H_2DCFDA (2′,7′-dichlorodihydrofluorescein diacetate), that allows to measure hydrogen peroxide (H_2O_2) and other radical oxidative species, and DHE (dihydroethidium), for superoxide anion ($O_2^{\bullet-}$) detection [61].

Cytosolic superoxide levels were evaluated in A549 cells treated with the imidazolyl-Pt(II) complexes at their corresponding IC_{50} values during 2 h by fluorescence measurements. As a result, only **[Pt-BFZ]** was able to significantly increased $O_2^{\bullet-}$ levels (Fig. 6A). These results were also confirmed by flow cytometry experiments (Fig. 6B) in which a dose dependent increase in the $O_2^{\bullet-}$ production was observed for **[Pt-BFZ]**, whereas **[Pt-MeIm]** and **[Pt-CTZ]** induce no effect even at two-fold the IC_{50} value.

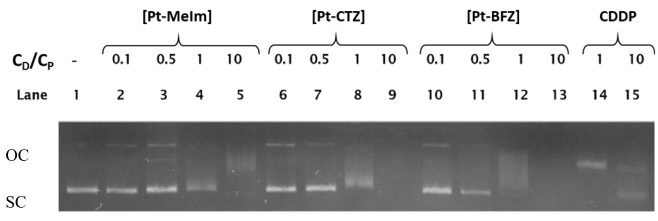

Fig. 5. Agarose electrophoresis of the plasmid DNA (pUC18) incubated overnight in the absence of Pt(II)-complexes (lane 1) and in the presence of different concentrations of [Pt-MeIm] (lanes 2–5), [Pt-CTZ] (lanes 6–9), [Pt-BFZ] (lanes 10–13) and CDDP (lanes 14 and 15). C_D/C_P stands for the Pt(II) complex/pUC18 concentrations ratio. Cisplatin (CDDP) was included as positive control.

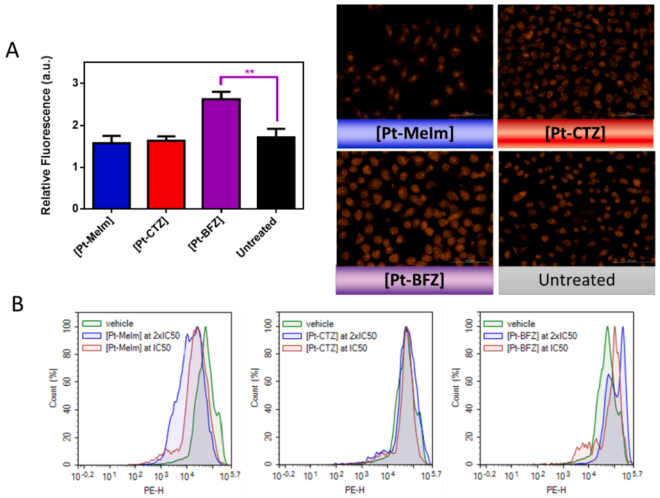

Fig. 6. Detection of superoxide anion by DHE after 2 h exposure of A549 cells to the imidazolyl-Pt(II) complexes. A) Relative fluorescence of treated cells at the IC_{50} values of the Pt(II) complexes relative to control cells. ** Statistical significance p-value <0.05 (t-test). B) Flow cytometry plots at the IC_{50} and 2-fold the IC_{50} values.

As afore-mentioned, to evaluate the generation of other ROS, A549 cells were treated with H_2DCFDA and with the Pt(II) complexes at their corresponding IC_{50} values or with TBH (*tert*-butyl hydroperoxide) as positive control during 4 h. **[Pt-CTZ]** do not induce significant differences in ROS levels compared to untreated cells (Fig. 7). By contrast, the generation ROS was clearly confirmed for **[Pt-MeIm]** and **[Pt-BFZ]**. Indeed, **[Pt-BFZ]** is the most potent H_2O_2 and other reactive oxygen species generator explaining is high cytotoxicity. Thus, the capacity of **[Pt-BFZ]** to induce oxidative stress seems to be the dominant factor in its anticancer activity. Therefore, a dual mechanism, that is to say covalent binding to DNA and ROS generation, could be responsible for the high cytotoxicity of **[Pt-MeIm]** and **[Pt-BFZ]**.

3.5.5. *Evaluation of mitochondrial membrane potential (MMP)*

The main source of intracellular ROS are the mitochondria, and their accumulation on them can alter mitochondria dynamics provoking mitochondria membrane depolarization, along with mitochondrial dysfunction and apoptosis triggered by the mitochondrial pathway. As a matter of fact, apoptosis induced by oxidative stress on mitochondria is a suitable approach for cancer treatment [62]. One of the effects of ROS generation may be the alteration of the mitochondrial membrane potential (MMP). So, we have evaluated changes of the MMP ($\Delta\Psi$) by using the tetramethyl rhodamine methyl ester (TMRM) probe, which is accumulated inside the mitochondria due to its cationic nature [63]. Treatment of A459 cells with **[Pt-CTZ]** seems to have no effect in MMP,

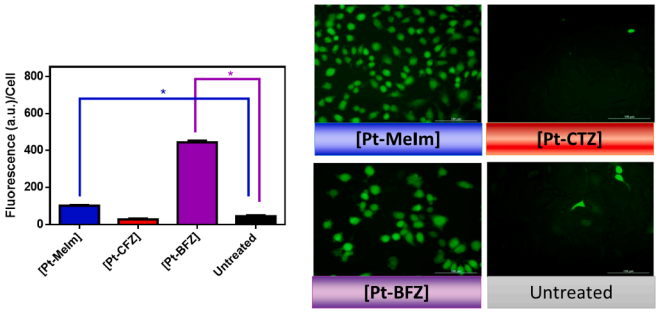

Fig. 7. Detection of ROS by H_2DCFDA after 4 h exposure of A549 cells to the imidazolyl-Pt(II) complexes. ** Statistical significance p-value <0.05 (ANOVA test with Dunnet's correction).

whereas **[Pt-BFZ]** led to a decreased in ΔΨ relative to vehicle-treated cells in a dose dependent manner (Fig. 8). Consequently, this ΔΨ is thought to affect both mitochondrial integrity and functionality. By contrast, the opposite trend is observed in cells treated with **[Pt-MeIm]**. The hyperpolarization of the mitochondrial membrane is larger as the concentration is increased, being extremely high at 2-fold the IC_{50} value. An enhanced ΔΨ indicates that the mitochondrial function is increased and a collapse in the mitochondria bioenergetics may occur.

3.5.6. *Cell cycle analysis*

Cell-cycle dysregulation is one of the prime features of cancer cells. Since cell cycle arrest renders tumor cells susceptible to apoptosis, targeting cell cycle phases and checkpoints is one promising approach in anticancer therapy [64]. Indeed, the cytotoxicity of many anticancer drugs is related to DNA damage and cell cycle perturbation [65]. To better understand the biological effect of the imidazolyl-Pt(II) complexes, the impact of these compounds at IC_{50} values on A549 cell cycle distribution was evaluated after 24 h of incubation time. The results indicated that complexes **[Pt-MeIm]** and **[Pt-BFZ]** lead to accumulation of treated cells at the G_0/G_1 phase (Fig. 9). Compared with the vehicle-treated control (DMSO), the percentage of cells in G_0/G_1 phase increased by 15.4% and 9.4% for **[Pt-MeIm]** and **[Pt-BFZ]**, respectively, while the number of cells in the S phase decreased accordingly. G_0/G_1 cell cycle arrest was previously described for several organometallic Pt(II) complexes [66] as well as for imidazole antifungal drugs, such as Clotrimazole, in some cancer cell lines [67,68,69]. By contrast, treatment with **[Pt-CTZ]** does not the block cell cycle progression.

3.5.7. *Apoptosis induction*

The ability of inducing apoptosis (programmed cell death) was evaluated for the Pt(II) complexes by flow cytometry using Annexin V staining, being this probe able to bind the anionic phospholipid phosphatidylserine in the cell surface of apoptotic cells [70]. The gathered results in Fig. 10 show that treatment of A549 cells with half the maximal inhibitory concentration of the Pt(II) complexes caused the highest accumulation in early apoptosis for **[Pt-BFZ]** and **[Pt-MeIm]**. In the case of **[Pt-CTZ]** treatment, similar amounts of cells in late apoptosis and necrosis were observed, while the percentage of cells in early apoptosis is smaller. Thus, the apoptosis induction pathway for **[Pt-CTZ]** may be different from that of **[Pt-BFZ]** and **[Pt-MeIm]**. The observed results suggest that **[Pt-BFZ]** and **[Pt-MeIm]** probably induce oxidative stress since ROS levels are increased and the MMP is affected. Hence, we speculate that apoptosis may be triggered by the mitochondrial pathway upon treatment with these two complexes.

4. Conclusion

In this work three neutral Pt(II) complexes containing imidazolyl drugs have been synthesized and characterized. The crystal structures of **[Pt-CTZ]** and **[Pt-BFZ]** have been resolved by X-Ray diffraction. These complexes exhibit high stability in water and in buffered solutions. The electronic and photophysical studies have shown that **[Pt-MeIm]** is phosphorescent in deoxygenated H_2O ($\tau_{1/2} = 3$ μs), whereas the other two cyclometalated Pt(II) complexes containing antifungal imidazolyl ligands, **[Pt-CTZ]** and **[Pt-BFZ]**, are also photoluminescent but exhibit lower excited state lifetimes. **[Pt-MeIm]** and **[Pt-BFZ]** present higher cytotoxicity than **[Pt-CTZ]** and cisplatin against colon adenocarcinoma (SW480), ovarian cancer (A2780) and lung adenocarcinoma (A549) cell lines. Despite their similar IC_{50} values, **[Pt-MeIm]** and **[Pt-BFZ]** feature dissimilar cellular uptake behaviors, **[Pt-MeIm]** is highly accumulated but **[Pt-BFZ]** is poorly internalized inside the cells after 24 h of incubation. Indeed, we postulate that the cellular uptake of the latter is strongly hindered by its interaction with plasma proteins. DNA may not be the main target for these complexes since all of them are able to interact with DNA by covalent binding inducing similar conformational changes on the DNA double helix, and the cytotoxicity of **[Pt-**

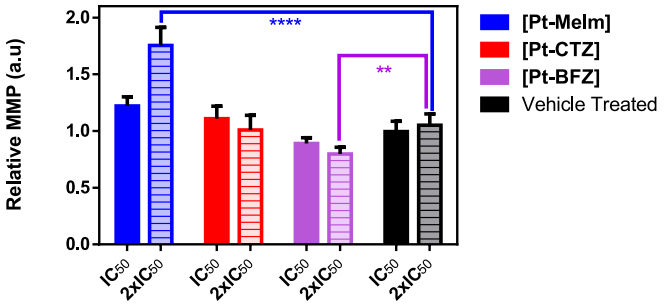

Fig. 8. Relative MMP (ΔΨ) of A549 cells treated with the Pt(II) complexes at their IC_{50} and 2-fold IC_{50} values relative to untreated cells. Vehicle treated (0.5% DMSO). Data were obtained from duplicates of two different experiments and plotted as mean values with standard deviation. **** (*p*-value <0.001) and ** (p-value <0.05) (ANOVA test with Dunnet's correction).

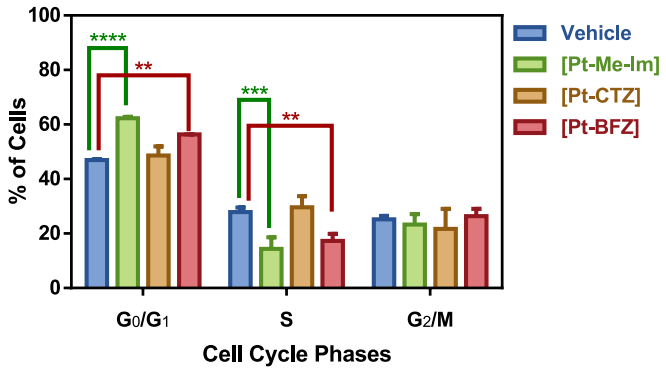

Fig. 9. A549 cells distribution in G_0/G_1, S and G_2/M phases upon treatment with the vehicle (0.5% DMSO) and the platinum complexes under study at the IC_{50} values. Data were obtained from duplicates of three different experiments and plotted as mean values with standard deviation. **** (*p*-value <0.0001) and *** (0.0001 ≥ p-value <0.001) extremely significant and ** (0.001 ≥ p-value <0.01) very significant differences (ANOVA test with Dunnet's correction).

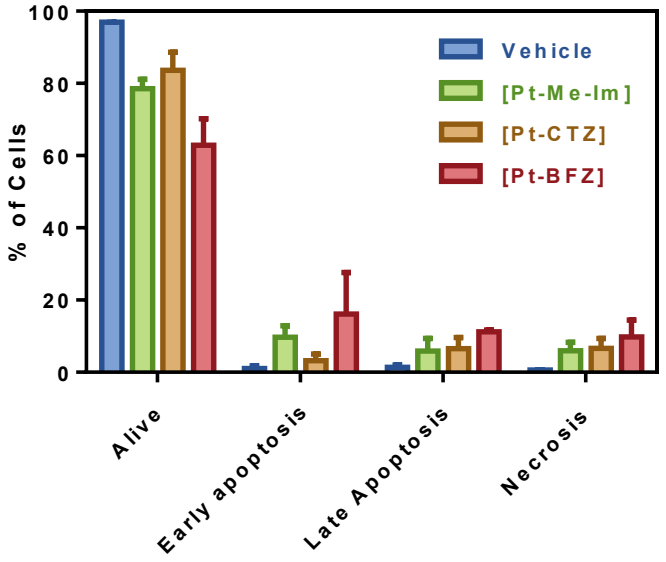

Fig. 10. Flow cytometry results expressed as percentage of A549 cells in alive, early apoptotic, late apoptotic and necrotic phases. Data were obtained from duplicates of two different experiments and plotted as mean values with standard deviation.

CTZ] is low. However, only **[Pt-MeIm]** and **[Pt-BFZ]** cause cell cycle perturbation with a significant accumulation of cells in G_0/G_1. Both induce changes in the mitochondrial membrane potential, and they seem to induce apoptosis by the mitochondrial pathway whereas the pathway of **[Pt-CTZ]** in apoptotic induction may be a different one. On the other hand, only **[Pt-MeIm]** and **[Pt-BFZ]** are able to cause ROS increase. The less accumulated, but high cytotoxic complex, **[Pt-BFZ]** shows a marked increase in ROS levels in comparison to **[Pt- MeIm]** . In fact, **[Pt-BFZ]** is the only derivative that increases $O_2^{\bullet-}$ levels. Thus, ROS generation seem to be the key for their biological activity.

Author Contributions

‡N. F—P and M. V. contributed equally. The manuscript was written through contributions of all authors. All authors have given approval to the final version of the manuscript.

Declaration of Competing Interest

The authors declare that they have no known competing financial interests or personal relationships that could have appeared to influence the work reported in this paper..

Acknowledgments

The authors gratefully acknowledge the financial support by La Caixa Foundation (LCF/PR/PR12/11070003), Consejería de Educación-Junta de Castilla y León-FEDER (BU042U16-BU305P18), Ministerio de Ciencia, Innovación y Universidades (RTI2018-102040-B-100). M.V. is grateful for the financial support received from the Consejería de Educación-Junta de Castilla y León-FEDER (BU042U16-BU305P18). We are indebted to P. Castroviejo and M. Mansilla (PCT of the Universidad de Burgos) for the technical support.

Appendix A. Supplementary data

Supplementary data to this article can be found online at https://doi.org/10.1016/j.jinorgbio.2021.111663.

References

[1] P.M. Buchel, W. Draber, E. Regel, Arzneimittelforschung 22 (1972) 1260–1272.
[2] J.M. Torres-Rodríguez, Arch. Med. Res. 24 (1993) 371–375.
[3] P.D. Crowley, H.C. Gallagher, J. Appl. Microbiol. 117 (2014) 611–617.
[4] S. Kadavakollu, C. Stailey, C.S. Kunapareddy, S. White, Med. Chem. 4 (2014) 722–724.
[5] J.S. Cheng, C.-T. Chou, W.-Z. Liang, C.-C. Kuo, P. Shieh, D.-H. Kuo, C.-R. Jan, J. Recept. Signal Transduct. 34 (2014) 449–493.
[6] J. Penso, R. Beitner, Eur. J. Pharmacol. 342 (1998) 113–117.
[7] T. Gagini, L. Colina-Vegas, W. Villarreal, L.P. Borba-Santos, C. De Souza Pereira, A. A. Batista, M. Kneip Fleury, W. De Souza, S. Rozental, L.A.S. Costa, et al., New J. Chem. 42 (2018) 13641–13650.
[8] R. Sánchez-Delgado, M. Navarro, K. Lazardi, R. Atencio, M. Capparelli, F. Vargas, J. Urbina, A. Bouillez, A.F. Noels, D. Masi, Acta 275–276 (1998) 528–540.
[9] M. Navarro, T. Lehmann, E.J. Cisneros-Fajardo, A. Fuentes, R.A. Sánchez-Delgado, P. Silva, J.A. Urbina, Polyhedron 19 (2000) 2319–2325.
[10] A. Martínez, T. Carreon, E. Iniguez, A. Anzellotti, A. Sánchez, M. Tyan, A. Sattler, L. Herrera, R.A. Maldonado, R.A. Sánchez-Delgado, J. Med. Chem. 55 (2012) 3867–3877.
[11] R.A. Sánchez-Delgado, K. Lazardi, L. Rincón, J.A. Urbina, A.J. Hubert, A.N. Noels, J. Med. Chem. (1993) 2041–2043.
[12] E. Iniguez, A. Varela-Ramirez, A. Martínez, C.L. Torres, R.A. Sánchez-Delgado, R. A. Maldonado, Acta Trop. 164 (2016) 402–410.
[13] J. Kljun, A.J. Scott, T. Lanišnik Rižner, J. Keiser, I. Turel, Organometallics 33 (2014) 1594–1601.
[14] L. Colina-Vegas, J. Lima Prado Godinho, T. Coutinho, R.S. Correa, W. De Souza, J. Cola Fernandes Rodrigues, A.A. Batista, M. Navarro, New J. Chem. 43 (2019) 1431–1439.
[15] E. Rodríguez Arce, C. Sarniguet, T.S. Moraes, M. Vieites, A.I. Tomaz, A. Medeiros, M.A. Comini, J. Varela, H. Cerecetto, M. González, F. Marques, M.H. García, L. Otero, D. Gambino, J. Coord. Chem. 68 (2015) 2923–2937.
[16] M. Navarro, I. Colmenares, H. Correia, A. Hernández, Y. Ching, Y. Millán, L. Ojeda, M. Velásquez, G. Fraile, Arzneimittelforschung 54 (2012) 746–751.
[17] E. Robles-Escajeda, A. Martínez, A. Varela-Ramirez, R.A. Sánchez-Delgado, R. J. Aguilera, Cell Biol. Toxicol. 29 (2013) 431–433.
[18] M. Strasberg Rieber, A. Anzellotti, R.A. Sánchez-Delgado, M. Rieber, Int. J. Cancer 112 (2004) 376–384.
[19] L. Colina-Vegas, J.L. Dutra, W. Villarreal, J.H. De A. Neto, M.R. Cominetti, F. Pavan, M. Navarro, A.A. Batista, J. Inorg. Biochem. 162 (2016) 135–145.
[20] M. Navarro, E.J. Cisneros-Fajardo, T. Lehmann, R.A. Sánchez-Delgado, R. Atencio, P. Silva, R. Lira, J.A. Urbina, Inorg. Chem. 40 (2001) 6879–6884.
[21] H.A. Mohamed, S. Shepherd, N. William, H.A. Blundell, M. Das, C.M. Pask, B.R. M. Lake, R.M. Phillips, A. Nelson, C.E. Willans, Organometallics 39 (2020) 1318–1331.
[22] M. Navarro, N.P. Peña, I. Colmenares, T. González, M. Arsenak, P. Taylor, J. Inorg. Biochem. 100 (2006) 152–157.
[23] P.V. Simpson, C. Nagel, H. Bruhn, U. Schatzschneider, Organometallics 34 (2015) 3809–3815.
[24] H.F. Abd El-Halim, F.A. Nour El-Dien, G.G. Mohamed, N.A. Mohmed, Synth. React. Inorganic, Met. Nano-Metal Chem. 41 (2011) 544–554.
[25] S. Betanzos-Lara, N.P. Chmel, M.T. Zimmerman, L.R. Barrón-Sosa, C. Garino, L. Salassa, A. Rodger, J.L. Brumaghim, I. Gracia-Mora, N. Barba-Behrens, Dalton Trans. 44 (2015) 3673–3685.
[26] S. Betanzos-Lara, C. Gómez-Ruiz, L.R. Barrón-Sosa, I. Gracia-Mora, M. Flores-Álamo, N. Barba-Behrens, J. Inorg. Biochem. 114 (2012) 82–93.
[27] V. Midlej, F. Rubim, W. Villarreal, É.S. Martins-Duarte, M. Navarro, W. de Souza, M. Benchimol, Parasitology 146 (2019) 1206–1216.
[28] M. Navarro, A.R. Higuera-Padilla, M. Arsenak, P. Taylor, Transit. Met. Chem. 34 (2009) 869–875.
[29] A. Annunziata, M.E. Cucciolito, R. Esposito, G. Ferraro, D.M. Monti, A. Merlino, F. Ruffo, Eur. J. Inorg. Chem. (2020) 918–929.
[30] G. Facchetti, I. Rimoldi, Bioorg. Med. Chem. Lett. 29 (2019) 1257–1263.
[31] M.V. Babak, M. Pfaffeneder-Kmen, S.M. Meier-Menches, M.S. Legina, S. Theiner, C. Licona, C. Orvain, M. Hejl, M. Hanif, M.A. Jakupec, B.K. Keppler, C. Gaiddon, C. G. Hartinger, Inorg. Chem. 57 (2018) 2851–2864.
[32] A.T. Dharmaraja, J. Med. Chem. 60 (2017) 3221–3240.
[33] B. Perillo, M. Di Donato, A. Pezone, E. Di Zazzo, P. Giovannelli, G. Galasso, G. Castoria, A. Migliaccio, Exp. Mol. Med. 52 (2020) 192–203.
[34] M. Vaquero, N. Busto, N. Fernández-Pampín, G. Espino, B. García, Inorg. Chem. 59 (2020) 4961–4971.
[35] M. Rothemund, S.I. Bär, T. Rehm, H. Kostrhunova, V. Brabec, R. Schobert, Dalton Trans. 49 (2020) 8901–8910.
[36] M. Clemente, I. Halil Polat, J. Albert, R. Bosque, M. Crespo, J. Granell, C. López, M. Martínez, J. Quirante, R. Messeguer, C. Calvis, J. Badía, L. Baldoma, M. Font-Bardia, M. Cascante, Organometallics *37* (**2018**) 3502–3514.
[37] SAINT Area-Detector Integr. Program, SAINT+ v7.12a, Bruker AXS Inc, Madison, WI, 2004.
[38] G.M. Sheldrick, SADABS A Progr. Empir. Absorpt. Correct. Version 2004/ 1, Univ. Gottingen, Gottingen, Germany, 2004.
[39] L. Farrugia, J. IUCr. WinGX and ORTEP for windows: an update, *J. Appl. Crystallogr.* 45 (2012) 849–854.
[40] O.V. Dolomanov, L.J. Bourhis, R.J. Gildea, J.A.K. Howard, H. Puschmann, J. Appl. Crystallogr. 42 (2009) 339–341.
[41] M. Martínez-Alonso, N. Busto, L.D. Aguirre, L. Berlanga, M.C. Carrión, J.V. Cuevas, A.M. Rodríguez, A. Carbayo, B.R. Manzano, E. Ortí, F.A. Jalón, B. García, G. Espino, Chem. Eur.J. 24 (2018) 17523–17537.
[42] H.M.E. Azzazy, R.H. Christenson, Clin. Chem. 43 (1997) 2014–2016.
[43] G. Felsenfeld, S.Z.A. Hirschman, S. Z. A., J. Mol. Biol. 13 (1965) 407–427.
[44] F. Niedermair, K. Waich, S. Kappaun, T. Mayr, G. Trimmel, K. Mereiter, C. Slugovc, Inorg. Chim. Acta 360 (2007) 2767–2777.
[45] A. Esmaeilbeig, H. Samouei, S. Abedanzadeh, Z. Amirghofran, J. Organomet. Chem. 696 (2011) 3135–3142.
[46] T. Okada, I.M. El-Mehasseb, M. Kodaka, T. Tomohiro, K. Okamoto, H. Okuno, J. Med. Chem. 44 (2001) 4661–4667.
[47] R.R. Parker, J.P. Sarju, A.C. Whitwood, J.A.G. Williams, J.M. Lynam, D.W. Bruce, Chem. – A Eur. J. 24 (2018) 19010–19023.
[48] N. Godbert, T. Pugliese, I. Aiello, A. Bellusci, A. Crispini, M. Ghedini, Eur. J. Inorg. Chem. (2007) 5105–5111.
[49] J.-Y. Cho, K.Y. Suponitsky, J. Li, T.V. Timofeeva, S. Barlow, S.R. Marder, J. Organomet. Chem. 690 (2005) 4090–4093.
[50] P.-I. Kvam, M.V. Puzyk, K.P. Balashev, Songstad, Acta Chem. Scand. 49 (1995) 335–343.
[51] D.M. Jenkins, J.F. Senn, S. Bernhard, Dalton Trans. 41 (2012) 8077–8085.
[52] S. Chen, R. Fn, X. Wang, Y. Yang, *Inorg. Chem. Commun.* 44 (2014) 101–106.
[53] S. Curry, *Drug Metab. Pharmacokinet.* 24 (2009) 342–357.
[54] G. Fanali, A. di Masi, V. Trezza, M. Marino, M. Fasano, P. Ascenzi, Mol. Asp. Med. 33 (2012) 209–290.
[55] J.J. Gullo, C.L. Litterst, P.J. Maguire, B.I. Sikic, D.F. Hoth, P.V. Woolley, Cancer Chemother. Pharmacol. 5 (1980) 21–26.
[56] D. Trachootham, J. Alexandre, P. Huang, Nat. Rev. Drug Discov. 8 (2009) 579–591.
[57] J. Li, X. He, Y. Zou, D. Chen, L. Yang, J. Rao, H. Chen, M.C.W. Chan, L. Li, Z. Guo, L.W. Zhang, C. Chen, Metallomics 9 (2017) 726–733.
[58] K.-B. Huang, F.-Y. Wang, H.-W. Feng, H. Luo, Y. Long, T. Zou, A.S.C. Chan, R. Liu, H. Zou, Z.-F. Chen, Y.-C. Liu, Y.-N. Liu, H. Liang, Chem. Commun. 55 (2019) 13066–13069.
[59] M.J.R. Tham, M.V. Babak, W. Ang, Angew. Chem. Int. Ed. 59 (2020) 19070–19078.
[60] B. Perillo, M. Di Donato, A. Pezone, E. Di Zazzo, P. Giovannelli, G. Galasso, G. Castoria, A. Migliaccio, Exp. Mol. Med. 52 (2020) 192–203.

[61] A. Wojtala, M. Bonora, D. Malinska, P. Pinton, J. Duszynski, M.R. Wieckowski, Methods to Monitor ROS Production by fluorescence microscopy and fluorometry. conceptual background and bioenergetic/mitochondrial aspects of oncometabolism, in: Methods in Enzymology 542, 2014, pp. 243–262. Ed. Elsevier Inc.
[62] C. Nguyen, S. Pandey, Cancer Cells 11 (2019) 916.
[63] S. Creed, M. McKenzie, Cancer Metabolism (2019) 69–76.
[64] D. Alimbetov, S. Askarova, B. Umbayev, T. Davis, D. Kipling, Int. J. Mol. Sci. 19 (2018) 1690.
[65] Z.A. Stewart, M.D. Westfall, J.A. Pietenpol, Trends Pharmacol. Sci. 24 (2003) 139–145.
[66] A. Zamora, S.A. Pérez, V. Rodríguez, C. Janiak, G.S. Yellol, J. Ruiz, J. Med. Chem. 58 (2015) 1320–1336.
[67] S.H. Bae, J.H. Park, H.G. Choi, S. Kim, H. Kim, Biomol. Ther. 26 (2018) 494–502.
[68] H. Liu, Y. Li, K.P. Raisch, K. P., Anti-Cancer Drugs 21 (2010) 841–849.
[69] B. Adinolfi, S. Carpi, A. Romanini, E. Da Pozzo, M. Castagna, B. Costa, C. Martini, S.-P. Olesen, N. Schmitt, M.C. Breschi, P. Nieri, S. Fogli, Anticancer Res. 35 (2015) 3781–3786.
[70] G. Zhang, V. Gurtu, S.R. Kain, G. Yan, BioTechniques 23 (1997) 525–531.